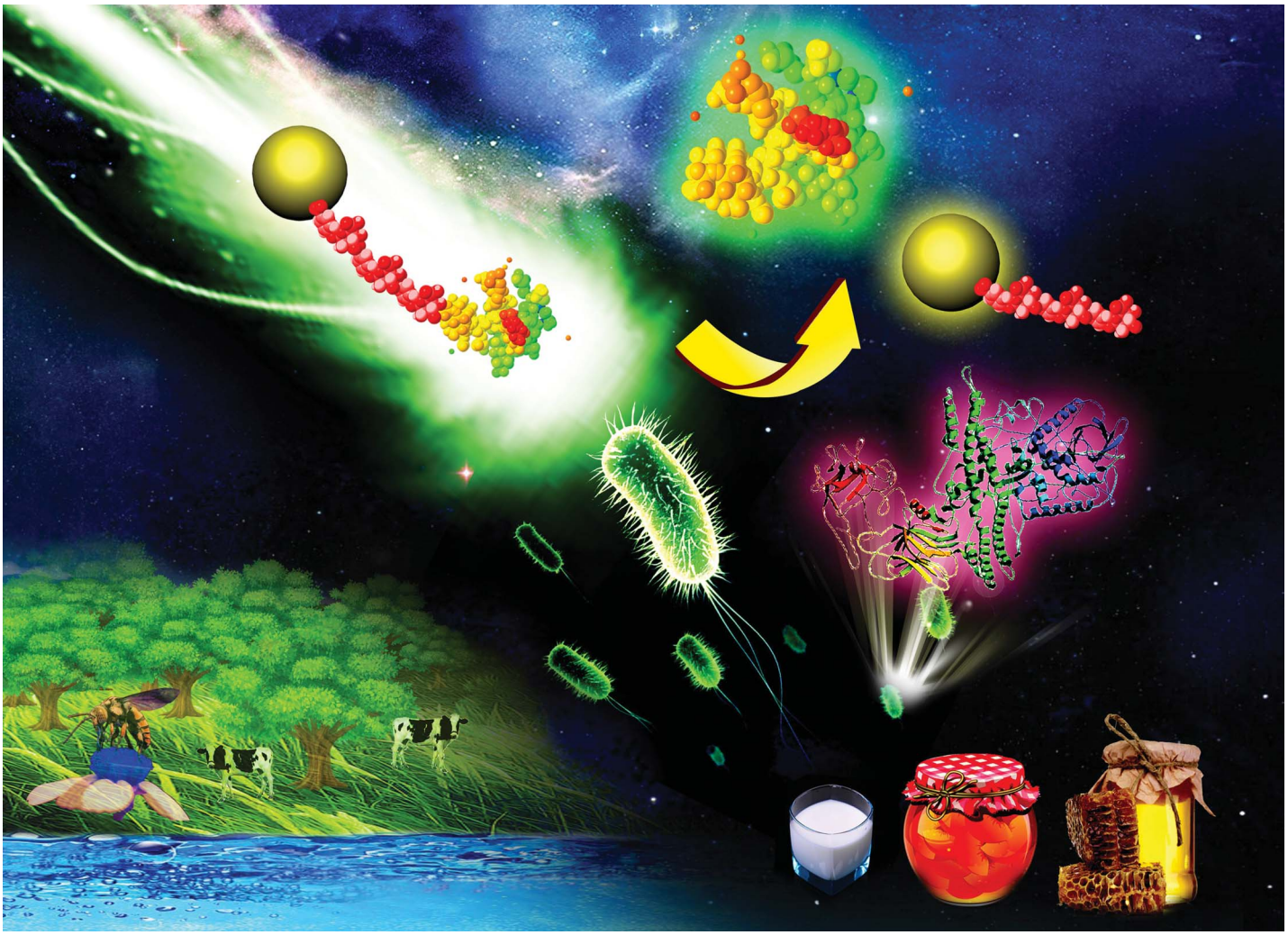

Showcasing research from Prof. Bo Liedberg's laboratory, at the Center for Biomimetic Sensor Science, School of Materials Science and Engineering, Nanyang Technological University, Singapore.

Time-resolved botulinum neurotoxin A activity monitored using peptide-functionalized Au nanoparticle energy transfer sensors

A fluorescence energy transfer sensor based on peptide-functionalized gold nanoparticles has been developed for sensitive (pM level) detection of botulinum neurotoxin A. The study specifically points out the importance of employing small "high curvature" nanoparticles to ensure favorable catalytic turn over rates.

As featured in:

See Bo Liedberg *et al.*, *Chem. Sci.*, 2014, **5**, 2651.

ROYAL SOCIETY OF CHEMISTRY

www.rsc.org/chemicalscience

Registered charity number: 207890

Chemical Science

EDGE ARTICLE

View Article Online
View Journal | View Issue

Cite this: *Chem. Sci.*, 2014, **5**, 2651

Time-resolved botulinum neurotoxin A activity monitored using peptide-functionalized Au nanoparticle energy transfer sensors†

Yi Wang,[ab] Xiaohu Liu,[a] Jinling Zhang,[ab] Daniel Aili[ac] and Bo Liedberg*[ab]

Received 3rd December 2013
Accepted 25th February 2014

DOI: 10.1039/c3sc53305k

www.rsc.org/chemicalscience

We report herein on the employment of synthetic peptide-functionalized gold nanoparticles (AuNPs) with various diameters as radiative quenchers for the time-resolved monitoring of botulinum A light chain (BoLcA) activity. The results demonstrate that larger AuNPs provide higher energy transfer efficiencies between the dye and the AuNPs, but poorer BoLcA activities for the proteolysis of peptides because of steric constraints. The initial turnover number for the BoLcA proteolysis of peptides on 18 nm AuNPs was retarded by a factor of 80 as compared with 1.4 nm AuNPs. A similar phenomenon has been observed for trypsin, however, with less hindrance on large AuNPs. Thus, the use of smaller 1.4 nm AuNPs in conjunction with robust synthetic peptides provides an attractive format for the time-resolved monitoring of protease activity and for BoLcA sensing at a highly competitive limit of detection (1 pM).

Introduction

Botulinum neurotoxins (BoNTs), produced by *Clostridium botulinum*,[1] are considered to be the most lethal substance known to humans. BoNTs are classified into seven immunologically distinct serotypes (A–G) each of which can cause flaccid muscle paralysis and subsequent death by blocking the release of neurotransmitters at neuromuscular junctions. Structurally, the neurotoxins are expressed as a single chain polypeptide which after post-translational proteolysis consists of two subunits: a 100 kDa heavy chain (HC) and a 50 kDa light chain (LC) linked *via* a disulfide bond. The HC is responsible for the binding and translocation of the toxin across the synaptic membrane through specific receptors; whereas the LC functions as an active zinc-endopeptidase that cleaves the SNARE (soluble *N*-ethylmaleimide-sensitive factor attachment protein receptor) proteins leading to the inhibition of acetylcholine release and subsequent neuroparalysis.[2] The neurotoxin can enter the body *via* the gastrointestinal tract or through mucous membranes of, for instance, the eyes or the respiratory tract. In humans, a lethal dose intravenously is estimated at 1–2 ng kg^{-1} body weight, orally at 1 μg kg^{-1} and 10–12 ng kg^{-1} by inhalation.[3] The gold standard "mouse bioassay" is able to detect as little as 10 pg ml^{-1} of toxin,[4] however, it requires several days of assay time, a large number of animals and can only be performed at specific laboratories. Therefore rapid, sensitive and easily accessible assays are required to meet biodefense diagnostic and therapeutic needs.

A number of *in vitro* assays to detect BoNTs, including ELISA,[5] immuno-PCR,[6] surface plasmon resonance (SPR) immunoassay[7] and electrochemical luminescence[8] have been developed.[9] However, these assays do not usually provide information on the enzymatic activity that is responsible for the toxicity of BoNTs. By rational design of a peptide substrate containing the BoNTs cleavage site derived from the SNARE protein, it is possible to monitor the activity of various serotypes of the BoNTs as each serotype cleaves at a different site on the SNARE protein. Assays to monitor the activity of BoNTs are typically based on measuring mass changes after the cleavage of the substrate *via* SPR;[10] counting the number of amplifiers or labels such as phage-based amplifiers,[11] or monitoring the reduction in the fluorescence resonance energy transfer (FRET) upon the cleavage of substrates.[12] Among these methods FRET has been extensively applied for the monitoring of proteolytic activities of various proteases including trypsin, caspase 1, caspase 3, thrombin, chymotrypsin, collagenase, HIV-1 protease and so on.[13] Several of the organic fluorophores commonly used in FRET bioassays suffer from pH sensitivity, photo-bleaching, chemical degradation and the overlapping of absorption spectra between the acceptor and donor. To address these problems, quantum dots (QDs) have been employed in FRET measurements because of their relative stability, tuneable emissions for the optimization of spectral overlap with a particular acceptor, and potential for minimization of the direct acceptor excitation.[14] However, the overlap between the emissions of the donor

[a]*Centre for Biomimetic Sensor Science, Nanyang Technological University, 50 Nanyang Drive, 637553 Singapore. E-mail: bliedberg@ntu.edu.sg; Tel: +65 6316 2957*

[b]*School of Materials Science and Engineering, Nanyang Technological University, 50 Nanyang Avenue, 639798 Singapore*

[c]*Division of Molecular Physics, Department of Physics, Chemistry and Biology, Linköping University, 58183 Linköping, Sweden*

† Electronic supplementary information (ESI) available: Details of experiments, FRET calculation, MALDI-TOF, DLS characterization and peptide-ratio dependent quenching efficiency of AuNPs. See DOI: 10.1039/c3sc53305k

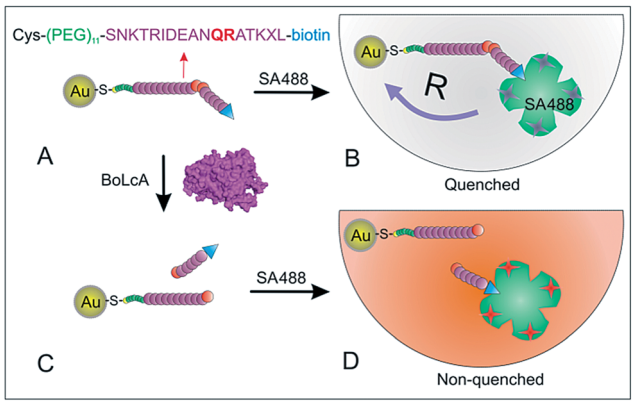

Fig. 1 Scheme showing the energy transfer between the peptide-functionalized AuNP and streptavidin–Alexa488 (SA488) before and after catalytic cleavage by BoLcA. (A) 1.4 nm AuNPs functionalized with a peptide substrate containing the BoLcA cleavage site (QR) and a terminal biotin. (B) Quenching of SA488 caused by the short distance R between dye and the AuNP surface. (C) Cleavage of the peptide on the AuNP by BoLcA. (D) Addition of SA488 to the suspension of the peptide-functionalized AuNPs after BoLcA cleavage.

and acceptor is still unavoidable, in addition to the potential toxicity of QDs.[15] Accordingly, having an acceptor that is non-fluorescent, such as metallic nanoparticles, can help to solve these issues. Metal nanoparticles have found applications either as radiative quenchers or radiative enhancers, depending on the particle size, shape, composition, and the distance between the donor and the metal nanoparticle.[16] For Au nanoparticles smaller than 40 nm in diameter, the absorption term dominates over the scattering term, and radiative quenching becomes the main cause for energy transfer from the dye to the metal which results in electron–hole pair formations and subsequent Ohmic losses.[16a] On the contrary, large nanoparticles are expected to enhance the fluorescence because scattering dominates over absorption. Au nanoparticles have been previously utilized as quenching beacons for the detection of DNA,[17] RNA,[18] proteases[19] and other biomolecules.[20]

In this paper, Au nanoparticles with diameters of 1.4 nm, 6 nm and 18 nm were modified with peptides containing a BoLcA cleavage site (AuNP–pep) and employed as radiative quenchers for monitoring the BoLcA activity. The AuNP–pep construct was pre-treated (cleaved) with BoLcA prior to incubation with the streptavidin–Alexa488 conjugate (SA488) to enable the measurement of the fluorescence intensity (Fig. 1). The fluorescence energy transfer efficiency was first investigated for AuNPs of different sizes. Then, the time-resolved catalytic activity of BoLcA on the AuNP–pep constructs was monitored and compared with the activity of trypsin on the same AuNP–pep construct. Finally, we employed the assay method shown in Fig. 1 for BoLcA sensing.

Results and discussion

Peptide sequence

Previous research has reported that a short peptide derived from the C-terminal end (187–203) of the SNAP-25 protein (part of the SNARE complex) can be hydrolyzed by BoNTs at a similar rate as the full length SNAP-25, as long as the peptide has a minimum length of 14 to 16 amino acids and arginine is present at the cleavage site.[21] The peptide sequence used in our study was based on the 17 amino acids at the C-terminus of the SNAP-25 protein (187–203). The glutamine–arginine (Q–R) located in the middle of the target peptide is the cleavage site for BoLcA proteolysis according to mass spectrometer results (Fig. S1†) and previous work.[21,22] Furthermore, substitution of methionine (M) in position 202 with norleucine (X) increases the proteolytic rate of BoLcA.[21,23] At the N-terminus of the peptide a cysteine was attached to enable its immobilization on the AuNPs *via* the –SH moiety.[24] In addition, an 11 unit ethylene glycol oligomer was introduced as a spacer between the Cys group and the recognition sequence to minimize the steric hindrance caused by the AuNPs. At the C-teriminus a biotin molecule was added to enable the specific interaction with the streptavidin–dye conjugate. SA488 contains 3–6 dyes per protein (see ESI†), which is advantageous compared with a single dye-labelled peptide, as it provides a higher fluorescence response to the peptide cleavage-induced dye release.

AuNP size-dependent energy transfer efficiency

The peptide was attached to AuNPs with diameters of 1.4, 6 and 18 nm (see experimental details in ESI and Fig. S2†) and their respective extinction spectra are shown in Fig. 2A. The 1.4 nm AuNPs displayed significantly lower extinction coefficients as compared with the 6 nm and 18 nm AuNPs because of their low electron density at the conduction band and large damping effect.[25] The 1.4 nm AuNP modified with the peptide substrate (AuNP–pep) was then incubated with SA488 at different molar ratios. The fluorescence intensity at $\lambda = 520$ nm decreased from $I_0 = 5.45 \times 10^5$ cps μA^{-1} for 10 nM SA488 to $I' = 2.0 \times 10^5$ cps μA^{-1} upon increasing the molar ratio of AuNP–pep : SA488 to 20 : 1 (Fig. 2B), and the energy transfer efficiency $E = 1 - I'/I_0$ became saturated at 62.5% for a AuNP–pep : SA488 ratio $\geq 5 : 1$ (Fig. 2C). The maximum fluorescence quenching efficiency was observed for a AuNP–pep : SA488 ratio of $\sim 5 : 1$ which is reasonable given that streptavidin has 4 affinity binding sites for biotins. Previous work suggests that small AuNPs with diameters of ~1–3 nm as acceptors can be described by the nanometal surface energy transfer (NSET) theory.[16a] In contrast to FRET, NSET does not require a resonant electronic transition as it originates from the interaction of the electromagnetic field of the donor dipole with the free conduction electrons of the accepting metal. The NSET characteristic distance R_0 is expressed as

$$R_0 = \left(0.225 \frac{c^3 \Phi_D}{\omega^2 \omega_f k_f}\right)^{1/4} \quad (1)$$

where c is the speed of light, Φ_D is the donor quantum efficiency, ω is the frequency of the donor electronic transition, ω_f and k_f are the Fermi frequency and Fermi wavevector of Au, respectively. In general, the fluorescence quenching efficiency E can be expressed as a function of the donor/acceptor distance, R, as

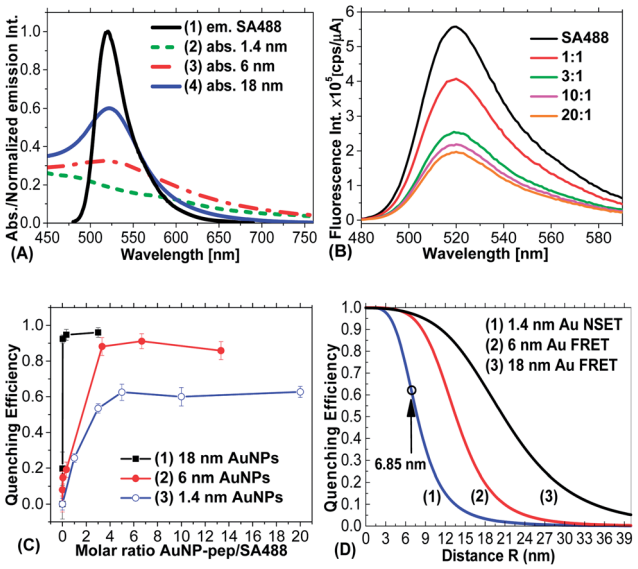

Fig. 2 (A) Normalized emission spectrum of (1) SA488 and absorption spectra of (2) 1.4 nm, (3) 6 nm and (4) 18 nm AuNP–pep. (B) Fluorescence spectra of 10 nM SA488 and following incubation with 1.4 nm AuNP–pep at AuNP–pep : SA488 ratios from 1 : 1 to 20 : 1. (C) Fluorescence quenching efficiency plotted as a function of the molar ratio of AuNP–pep : SA488 with AuNP diameters of (1) 18 nm, (2) 6 nm and (3) 1.4 nm. (D) Simulated fluorescence quenching efficiency *versus* the distance between the dyes and the surface of the AuNPs with diameters of (1) 1.4 nm, (2) 6 nm and (3) 18 nm based on NSET, FRET and FRET, respectively.

$$E = \frac{1}{1 + (R/R_0)^n} \quad (2)$$

where $n = 6$ for FRET and $n = 4$ for NSET. The NSET radius (R_0) is calculated to equal $R_0 = 7.78$ nm, according to eqn (1) by using the quantum efficiency of Alexa Fluor 488 $\Phi_D = 0.8$, $\omega = 3.63 \times 10^{15}$ s^{-1}, $\omega_f = 8.4 \times 10^{15}$ s^{-1} and $k_f = 1.2 \times 10^8$ cm^{-1}. Note that R is the distance between the molecular donor center and the Au surface for NSET, while for FRET, R is the distance between the donor center and the center of the Au nanoparticles. The distance dependent fluorescence quenching efficiency (eqn (2)) is plotted in Fig. 2D, from which the distance between the dye and AuNPs was estimated as $R = 6.85$ nm in the case of the 1.4 nm AuNP–pep constructs based on NSET. The distance is shorter than the linear extension length of the peptide $L \sim 8$ nm which might indicate that the immobilized peptide adopts a slightly bent or folded structure.

As compared with 1.4 nm AuNPs, the larger AuNPs, with diameters of 6 nm and 18 nm, displayed increased fluorescence quenching efficiencies (Fig. 2C). The fluorescence quenching efficiencies for 6 nm and 18 nm AuNPs reached a maximum of around 90% and 98% for molar ratios of 3 : 1 and 1 : 3, respectively. This is reasonable as the large AuNPs offer higher extinction coefficients and carry a larger number of peptides. The 1.4 nm AuNPs were modified with a single maleimide group for the attachment of one peptide per AuNP (see ESI†). The average number of peptides on each 18 nm and 6 nm AuNP was estimated to be 51 and 3, respectively. This estimation is based on a peptide/thiol-PEG molar ratio of 1 : 100 (18 nm AuNPs) and 0.5 : 100 (6 nm AuNPs), respectively, and the assumption that each thiol occupies an area of 0.2 nm^2. These observations, shown in Fig. 2, suggest that the fluorescence quenching efficiency is determined by both the size of the AuNPs, and the coverage of peptides on the AuNPs. The fluorescence quenching efficiency reached a maximum at a lower AuNP–pep : SA488 ratio when the coverage of peptide on 6 nm AuNPs was increased (Fig. S3†). Furthermore, the energy transfer for large AuNPs with diameters of 6 nm and 18 nm was assumed to be dominated by FRET, from which the characteristic radius (R_0) was estimated as $R_0 = 16.6$ and 29.8 nm, respectively (see ESI†). Accordingly, based on the calculation that the distance between the dye and the AuNP surface is about $R = 6.85$ nm, we estimate a quenching efficiency of $E \sim 95\%$ and 98% for the 6 and 18 nm AuNPs, respectively (eqn (2)). These values are consistent with the maximum fluorescence quenching efficiencies of $E = 92\%$ and 98% for the 6 and 18 nm AuNPs, respectively, as presented in Fig. 2C. Thus, our results confirm that the energy transfer on AuNPs with a diameter larger than 6 nm follows the FRET mechanism. One can of course argue that there is always a risk for aggregation between AuNPs induced by the multivalency of streptavidin (4 binding pockets per molecule). This might occur when there is more than one peptide per AuNP (as for the 6 and 18 nm particles). However, no colour change nor any plasmon band shift were observed after mixing SA488 with the 6 nm AuNPs at the molar ratio of AuNP–pep : SA488 of 3 : 1, indicating negligible aggregation of the AuNPs (Fig. S4†).

AuNPs size-dependent protease activity

The BoLcA activity was monitored through time-dependent fluorescence spectra of SA488 incubated with 1.4 nm AuNP–peps which were pre-treated with BoLcA for 30 min to 6 hours (Fig. 3A). The fluorescence intensity at the emission wavelength of 520 nm increased from 2.2×10^5 to 3.2×10^5 cps μA^{-1} after a 0.5 h incubation with 10 nM BoLcA and reached saturation at 4.0×10^5 cps μA^{-1} after a 2 h incubation.

The time-dependent peptide cleavage for AuNPs with diameters of 1.4 nm, 6 nm and 18 nm is demonstrated in Fig. 3B. The kinetics show saturation in 2 to 5 hours for the 1.4 nm AuNP–pep (200 nM) after exposure to 3 nM and 10 nM BoLcA, with an initial catalytic rate $v = 0.6$ nM min^{-1} and 2 nM min^{-1}, respectively. This corresponds to an initial turnover number of $k = 0.2$ min^{-1}. The corresponding initial turnover number for 6 nm and 18 nm AuNPs is 0.0025 min^{-1}, which is 80-fold lower than that for the 1.4 nm AuNPs. The k values were calculated based on a coverage of 3 peptides per 6 nm AuNP (12 nM) and 51 peptides per 18 nm AuNP (1 nM) which were cleaved initially at a rate of 0.78 and 0.75 peptides per hour with 5 nM BoLcA, respectively. The rate constant is calculated as $K_T = k_{cat}/K_M$ and equals 2.8×10^6 M^{-1} min^{-1} (see Fig. 3D and details in ESI†), based on the fitting of the kinetics for 1.4 nm AuNP–pep incubation with 3 nM and 10 nM BoLcA. Assuming $k_{cat} = 30$ s^{-1} as reported with the same peptide sequence,[21] the Michaelis–Menten constant K_M is estimated to equal $K_M = 643$ μM, which is comparable to that of the free peptide.[21] The poorer activity of

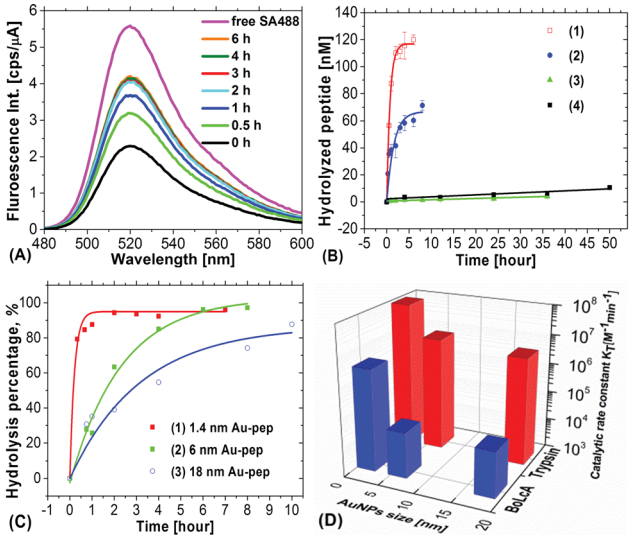

Fig. 3 (A) Evolution of the fluorescence intensity upon SA488 interaction with 1.4 nm AuNP–pep pre-incubated with 10 nM BoLcA for 0 to 6 hours at 37 °C. (B) The time-dependent evolution of peptide hydrolysis measured for 1.4 nm AuNP-pep treated with (1) 10 nM BoLcA and (2) 3 nM BoLcA, and (3) 6 nm and (4) 18 nm AuNP-pep treated with 5 nM BoLcA. (C) The time-dependent evolution of peptide hydrolysis measured for (1) 1.4 nm, (2) 6 nm and (3) 18 nm AuNP–pep which were pretreated with 1 nM trypsin. (D) The size-dependent protease rate constant K_T of trypsin and BoLcA on 1.4 nm, 6 nm and 18 nm AuNP–pep.

BoLcA for the peptide on the large AuNPs is ascribed to the fact that the active pocket of BoLcA is deeply buried inside the enzyme (~2.4 nm),[26] and steric hindrance induced by the AuNPs.

A similar phenomenon was also observed for trypsin and the same AuNP–pep. The catalytic rate of trypsin was higher for small AuNPs than for large AuNPs as indicated in Fig. 3C. The cleavage percentage was defined as $\Delta F/(F_{SA488} - F_0)$, where F_{SA488} and F_0 are the fluorescence intensities of free SA488 and AuNP–pep : SA488 conjugates measured at $\lambda = 520$ nm, respectively. The results indicated that about 90% of peptides on AuNPs were hydrolyzed by trypsin after 1, 4 and 10 hours for 1.4 nm, 6 nm and 18 nm AuNP–pep, respectively. As compared with BoLcA (Fig. 3B), trypsin hydrolyzed a higher amount of peptide in a shorter reaction time, indicating a higher activity. The rate constant K_T was estimated as $K_T = 8.1 \times 10^7$ M^{-1} min^{-1}, 7.2×10^6 M^{-1} min^{-1} and 4.42×10^6 M^{-1} min^{-1} for the AuNPs with diameters of 1.4 nm, 6 nm and 18 nm, respectively (Fig. 3D). The K_T values are comparable to previously reported values 7.8×10^7–2.34×10^8 M^{-1} min^{-1} for the digestion of a fifteen-residue peptide substrate by trypsin,[27] but 3 orders of magnitude higher than that reported for four-residue peptide substrates containing an arginine cleavage site.[28] The trypsin proteolytic activity is about 29 times higher than that of BoLcA. Furthermore, upon increasing the size of AuNPs from 1.4 nm to 18 nm in diameter, the trypsin activity decreased by 18 fold, a decrease that was 4 times smaller than the 80-fold decrease for BoLcA (Fig. 3D). Again the poor catalytic activity of BoLcA and more significant hindrance by large AuNPs might be ascribed to the deeper active pocket sites and 2-fold higher molecular weight of BoLcA as compared to trypsin, as well as the smaller number of cleavage sites provided by the peptide substrate. There are 4 trypsin cleavage sites in total (*i.e.* lysine K and arginine R) and only one (QR) for BoLcA.

BoLcA sensing

Considering the situation that the large AuNPs significantly hindered the accessibility of BoLcA to the peptides on the surface, we employed the smallest AuNPs (*i.e.* 1.4 nm in diameter) for the detection of BoLcA. The time-dependent fluorescence intensity of SA488 was monitored after incubation with AuNP–pep which was pre-treated with BoLcA at various concentrations from 1 pM to 10 nM at 37 °C (Fig. 4A). The fluorescence intensity saturated quickly after 2 hours incubation of AuNP–pep with BoLcA at concentrations higher than 3 nM (Fig. 4A). However, at low concentrations of BoLcA (<3 nM), the fluorescence intensity increased at an approximately constant rate after 2 hours of incubation. It is interesting to note that at concentrations of BoLcA lower than 3 nM the fluorescence intensity decreased in the first reaction hour (see insert in Fig. 4A). This might tentatively be ascribed to a transient conformational change of the peptide upon favourable interaction with BoLcA prior to cleavage. This hypothesis is based on the assumption that the fluorescence decline is due to

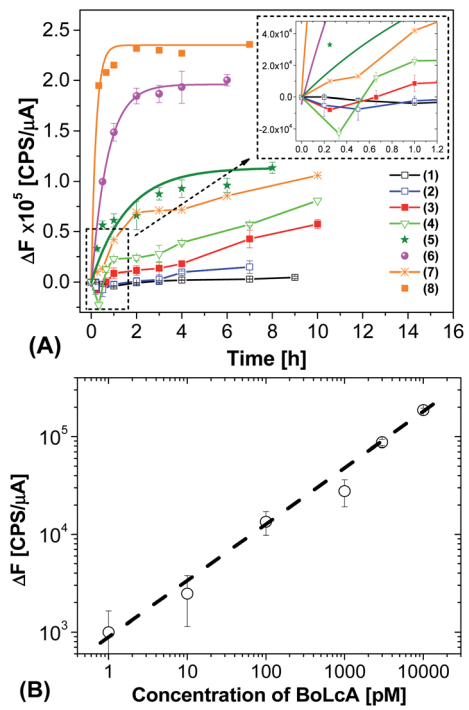

Fig. 4 (A) The time-dependent fluorescence intensity changes ΔF of SA488 on 1.4 nm AuNP–pep pretreated with (1) 1 pM, (2) 10 pM, (3) 100 pM, (4) 1 nM, (5) 3 nM and (6) 10 nM BoLcA, and (7) 10 pM and (8) 1 nM trypsin. (B) The calibration curve for the detection of BoLcA corresponding to the response at 2 hours from the incubation data in (A).

a decrease in the distance between the dye and the AuNP. The same trend was not observed for trypsin at concentrations down to 1 pM because of its higher catalytic rate and its less deep catalytic/cleavage site compared to BoLcA (Fig. 3D and 4A). However, to confirm whether the peptide changes conformation upon affinity interaction with BoLcA will require more advanced single-molecule measurements,[29] experiments that are beyond the scope of the present study.

The calibration curve for the detection of BoLcA from 1 pM to 10 nM reveals a limit of detection (LOD) of 1 pM (50 pg ml^{-1}), which is determined as the concentration of BoLcA at which the fluorescence intensity change ΔF is three times the standard deviation of the fluorescence fluctuation of the control samples, *i.e.* $3 \times \Delta F = 1000$ cps μA^{-1}. The method enabled the sensitive detection of BoLcA with an assay time of 2–3 hours which is comparable to the vesicle amplified SPR sandwich assay (LOD ~0.3 to 10 pM and assay time of 10 min to several hours),[10] aptamer-based electrochemical assay (LOD of 40 pg ml^{-1} and assay time of 24 h),[30] and the antibody-based SPR sandwich assay for the detection of BoNT Type B in buffer and honey (LOD ~ 2 pM and assay time of 1–2 h).[7] The LOD is about 2 to 3 orders of magnitude lower than the quantum dots-based FRET method (LOD ~ 350 pM and assay time of 2–3 h),[31] antibody-based ELISA (LOD of 0.2–2 ng ml^{-1} and assay time of 8 h).[5] But it is less sensitive than mouse lethality assay (LOD of 20–30 pg ml^{-1} and assay time of 2–4 days).[32] However, our method typically provides a shorter assay time than that of conventional ELISA and mouse lethality assays, and is expected to be a more robust assay than the antibody-based assays.

Conclusion

We have designed and synthesized a substrate peptide, which was immobilized on AuNPs with diameters of 1.4–18 nm, for the detection of BoLcA activity using a fluorescence energy transfer assay format. The results indicated that larger AuNPs provided higher quenching efficiencies, but significantly hindered the accessibility of BoLcA to the peptides on the AuNP surface, thus leading to an 80-fold lower initial catalytic rate for BoLcA. The assay exhibited a limit of detection of 1 pM for the detection of BoLcA with an assay time of 2–3 hours which is faster and more sensitive than many other assays including conventional ELISA. The proposed assay, based on a synthetic peptide, is also more robust than antibody-based assays.

Acknowledgements

This research is supported by the Science & Engineering Research Council (SERC) of the Agency for Science, Technology and Research (A*STAR), for projects under the number 1021520015.

References

1 C. Montecucco and J. Molgo, *Curr. Opin. Pharmacol.*, 2005, **5**, 274–279.
2 (*a*) B. R. Singh, *Neurotoxic. Res.*, 2006, **9**, 73–92; (*b*) G. Schiavo, M. Matteoli and C. Montecucco, *Physiol. Rev.*, 2000, **80**, 717–766; (*c*) L. Li and B. R. Singh, *J. Toxicol., Toxin Rev.*, 1999, **18**, 95–112.
3 S. S. Arnon, R. Schechter, T. V. Inglesby, D. A. Henderson, J. G. Bartlett, M. S. Ascher, E. Eitzen, A. D. Fine, J. Hauer, M. Layton, S. Lillibridge, M. T. Osterholm, T. O'Toole, G. Parker, T. M. Perl, P. K. Russell, D. L. Swerdlow, K. Tonat and W. G. C. Biodefense, *JAMA, J. Am. Med. Assoc.*, 2001, **285**, 1059–1070.
4 S. K. Sharma and R. C. Whiting, *J. Food Prot.*, 2005, **68**, 1256–1263.
5 (*a*) M. A. Poli, V. R. Rivera and D. Neal, *Toxicon*, 2002, **40**, 797–802; (*b*) M. Szilagyi, V. R. Rivera, D. Neal, G. A. Merrill and M. A. Poli, *Toxicon*, 2000, **38**, 381–389.
6 (*a*) J. T. Mason, L. X. Xu, Z. M. Sheng and T. J. O'Leary, *Nat. Biotechnol.*, 2006, **24**, 555–557; (*b*) J. T. Mason, L. Xu, Z. M. Sheng, J. He and T. J. O'Leary, *Nat. Protoc.*, 2006, **1**, 2003–2011; (*c*) H. C. Wu, Y. L. Huang, S. C. Lai, Y. Y. Huang and M. F. Shalo, *Lett. Appl. Microbiol.*, 2001, **32**, 321–325.
7 J. Ladd, A. D. Taylor, J. Homola and S. Y. Jiang, *Sens. Actuators, B*, 2008, **130**, 129–134.
8 (*a*) V. R. Rivera, F. J. Gamez, W. K. Keener, J. A. White and M. A. Poli, *Anal. Biochem.*, 2006, **353**, 248–256; (*b*) V. Guglielmo-Viret, O. Attree, V. Blanco-Gros and P. Thullier, *J. Immunol. Methods*, 2005, **301**, 164–172.
9 J. W. Grate, R. M. Ozanich, M. G. Warner, J. D. Marks and C. J. Bruckner-Lea, *TrAC, Trends Anal. Chem.*, 2010, **29**, 1137–1156.
10 G. Ferracci, S. Marconi, C. Mazuet, E. Jover, M. P. Blanchard, M. Seagar, M. Popoff and C. Leveque, *Anal. Biochem.*, 2011, **410**, 281–288.
11 P. Capek, K. S. Kirkconnell and T. J. Dickerson, *J. Am. Chem. Soc.*, 2010, **132**, 13126–13128.
12 (*a*) S. Sun, J. Francis, K. E. Sapsford, Y. Kostov and A. Rasooly, *Sens. Actuators, B*, 2010, **146**, 297–306; (*b*) D. Min, W. H. Tepp, E. A. Johnson and E. R. Chapman, *Proc. Natl. Acad. Sci. U. S. A.*, 2004, **101**, 14701–14706; (*c*) J. J. Schmidt, R. G. Stafford and C. B. Millard, *Anal. Biochem.*, 2001, **296**, 130–137; (*d*) J. A. Ross, M. A. Gilmore, D. Williams, K. R. Aoki, L. E. Steward and D. M. Jameson, *Anal. Biochem.*, 2011, **413**, 43–49.
13 (*a*) Y. Choi, J. Lee, K. Kim, H. Kim, P. Sommer and R. Song, *Chem. Commun.*, 2010, **46**, 9146–9148; (*b*) Y. H. Wang, P. Shen, C. Y. Li, Y. Y. Wang and Z. H. Liu, *Anal. Chem.*, 2012, **84**, 1466–1473; (*c*) T. Zauner, R. Berger-Hoffmann, K. Muller, R. Hoffmann and T. Zuchner, *Anal. Chem.*, 2011, **83**, 7356–7363; (*d*) J. Karvinen, V. Laitala, M. L. Makinen, O. Mulari, J. Tamminen, J. Hermonen, P. Hurskainen and I. Hemmila, *Anal. Chem.*, 2004, **76**, 1429–1436; (*e*) D. E. Prasuhn, A. Feltz, J. B. Blanco-Canosa, K. Susumu, M. H. Stewart, B. C. Mei, A. V. Yakovlev, C. Loukov, J. M. Mallet, M. Oheim, P. E. Dawson and I. L. Medintz, *ACS Nano*, 2010, **4**, 5487–5497.
14 (*a*) I. L. Medintz, A. R. Clapp, F. M. Brunel, T. Tiefenbrunn, H. T. Uyeda, E. L. Chang, J. R. Deschamps, P. E. Dawson

and H. Mattoussi, *Nat. Mater.*, 2006, **5**, 581–589; (*b*) K. Boeneman, B. C. Mei, A. M. Dennis, G. Bao, J. R. Deschamps, H. Mattoussi and I. L. Medintz, *J. Am. Chem. Soc.*, 2009, **131**, 3828–3829; (*c*) H. Q. Yao, Y. Zhang, F. Xiao, Z. Y. Xia and J. H. Rao, *Angew. Chem., Int. Ed.*, 2007, **46**, 4346–4349; (*d*) L. F. Shi, V. De Paoli, N. Rosenzweig and Z. Rosenzweig, *J. Am. Chem. Soc.*, 2006, **128**, 10378–10379; (*e*) W. R. Algar, A. Malonoski, J. R. Deschamps, J. B. Banco-Canosa, K. Susumu, M. H. Stewart, B. J. Johnson, P. E. Dawson and I. L. Medintz, *Nano Lett.*, 2012, **12**, 3793–3802.

15 (*a*) R. Hardman, *Environ. Health Perspect.*, 2006, **114**, 165–172; (*b*) M. Bottrill and M. Green, *Chem. Commun.*, 2011, **47**, 7039–7050; (*c*) L. Y. T. Chou and W. C. W. Chan, *Nat. Nanotechnol.*, 2012, **7**, 416–417.

16 (*a*) M. P. Singh and G. F. Strouse, *J. Am. Chem. Soc.*, 2010, **132**, 9383–9391; (*b*) T. L. Jennings, M. P. Singh and G. F. Strouse, *J. Am. Chem. Soc.*, 2006, **128**, 5462–5467; (*c*) J. R. Lakowicz, *Anal. Biochem.*, 2005, **337**, 171–194; (*d*) T. Pons, I. L. Medintz, K. E. Sapsford, S. Higashiya, A. F. Grimes, D. S. English and H. Mattoussi, *Nano Lett.*, 2007, **7**, 3157–3164; (*e*) Y. Wang, L. Wu, X. D. Zhou, T. I. Wong, J. L. Zhang, P. Bai, E. P. Li and B. Liedberg, *Sens. Actuators, B*, 2013, **186**, 205–211.

17 (*a*) B. Dubertret, M. Calame and A. J. Libchaber, *Nat. Biotechnol.*, 2001, **19**, 365–370; (*b*) H. Wang, J. S. Li, Y. X. Wang, J. Y. Jin, R. H. Yang, K. M. Wang and W. H. Tan, *Anal. Chem.*, 2010, **82**, 7684–7690; (*c*) F. Li, H. Pei, L. H. Wang, J. X. Lu, J. M. Gao, B. W. Jiang, X. C. Zhao and C. H. Fan, *Adv. Funct. Mater.*, 2013, **23**, 4140–4148.

18 (*a*) D. S. Seferos, D. A. Giljohann, H. D. Hill, A. E. Prigodich and C. A. Mirkin, *J. Am. Chem. Soc.*, 2007, **129**, 15477–15479; (*b*) J. P. Xue, L. L. Shan, H. Y. Chen, Y. Li, H. Y. Zhu, D. W. Deng, Z. Y. Qian, S. Achilefu and Y. Q. Gu, *Biosens. Bioelectron.*, 2013, **41**, 71–77; (*c*) N. Li, C. Y. Chang, W. Pan and B. Tang, *Angew. Chem., Int. Ed.*, 2012, **51**, 7426–7430.

19 (*a*) Y. P. Kim, Y. H. Oh, E. Oh, S. Ko, M. K. Han and H. S. Kim, *Anal. Chem.*, 2008, **80**, 4634–4641; (*b*) D. W. Deng, D. Y. Zhang, Y. Li, S. Achilefu and Y. Q. Gu, *Biosens. Bioelectron.*, 2013, **49**, 216–221.

20 (*a*) D. Zheng, D. S. Seferos, D. A. Giljohann, P. C. Patel and C. A. Mirkin, *Nano Lett.*, 2009, **9**, 3258–3261; (*b*) X. Y. Huang, T. Lan, B. C. Zhang and J. C. Ren, *Analyst*, 2012, **137**, 3659–3666.

21 J. J. Schmidt and K. A. Bostian, *J. Protein Chem.*, 1997, **16**, 19–26.

22 X. Liu, Y. Wang, P. Chen, Y. Wang, J. Zhang, D. Aili and B. Liedberg, *Anal. Chem.*, 2014, **86**, 2345–2352.

23 J. J. Schmidt and K. A. Bostian, *J. Protein Chem.*, 1995, **14**, 703–708.

24 P. Chen, R. Selegard, D. Aili and B. Liedberg, *Nanoscale*, 2013, **5**, 8973–8976.

25 S. Link and M. A. El-Sayed, *Int. Rev. Phys. Chem.*, 2000, **19**, 409–453.

26 R. Kukreja and B. R. Singh, in *Microbial Toxins: Current Research and Future Trends*, Caister Academic Press, 2009.

27 G. S. Coombs, M. S. Rao, A. J. Olson, P. E. Dawson and E. L. Madison, *J. Biol. Chem.*, 1999, **274**, 24074–24079.

28 R. M. Caprioli and L. Smith, *Anal. Chem.*, 1986, **58**, 1080–1083.

29 X. Michalet, S. Weiss and M. Jager, *Chem. Rev.*, 2006, **106**, 1785–1813.

30 F. Wei and C. M. Ho, *Anal. Bioanal. Chem.*, 2009, **393**, 1943–1948.

31 K. E. Sapsford, J. Granek, J. R. Deschamps, K. Boeneman, J. B. Blanco-Canosa, P. E. Dawson, K. Susumu, M. H. Stewart and I. L. Medintz, *ACS Nano*, 2011, **5**, 2687–2699.

32 M. Lindstrom and H. Korkeala, *Clin. Microbiol. Rev.*, 2006, **19**, 298–314.

